

Project AutoVision: Localization and 3D Scene Perception for an Autonomous Vehicle with a Multi-Camera System

Lionel Heng¹, Benjamin Choi¹, Zhaopeng Cui², Marcel Geppert², Sixing Hu⁴, Benson Kuan¹, Peidong Liu², Rang Nguyen⁴, Ye Chuan Yeo¹, Andreas Geiger³, Gim Hee Lee⁴, Marc Pollefeys², and Torsten Sattler²

Abstract—Project AutoVision aims to develop localization and 3D scene perception capabilities for a self-driving vehicle and which will enable autonomous navigation in urban and rural environments, in day and night, and with cameras as the only exteroceptive sensors. The sensor suite employs many cameras for both 360-degree coverage and accurate multi-view stereo; the use of low-cost cameras keeps the cost of this sensor suite to a minimum. In addition, the project seeks to extend the operating envelope to include GNSS-less conditions which are typical for environments with tall buildings, foliage, and tunnels. Emphasis is placed on marrying multi-view geometry with deep learning to enable the vehicle to localize and perceive in 3D space. This paper presents an overview of the project, and describes the sensor suite and current progress in the areas of calibration, localization, and perception.

I. INTRODUCTION

The three DARPA Grand Challenges in the last decade set off a wave of disruption in the automotive industry. With widespread belief that autonomous vehicles can revolutionize logistics and mobility, automakers and technology companies are racing with one another to put autonomous vehicles on the road within the next few years. LiDAR sensors are the primary sensing modality for a vast majority of autonomous vehicles; they generate highly accurate 3D point cloud data in both day and night, and enable localization and 3D scene perception at all times of the day. In contrast, cameras require sufficient ambient lighting, and do not directly provide 3D point cloud data. However, cameras yield high-resolution image data which better facilitates scene segmentation and understanding. In addition, we can leverage multi-view geometry techniques to infer depth data from multiple cameras albeit with lower accuracy than depth data from LiDAR sensors. Cameras can be fitted with either wide-field-of-view or fisheye lenses, giving them a significantly larger vertical field of view and higher vertical resolution compared to LiDAR sensors.

Project AutoVision started in late 2016 with the goal to develop localization and 3D scene perception algorithms for autonomous vehicles exclusively equipped with cameras. Project AutoVision is similar to, but differs from Project V-Charge [8, 27, 11] in the aspect that Project AutoVision extends the operating envelope from parking lots and garages to urban and rural environments with widely varying illumination conditions. We work towards real-time 3D map-



Fig. 1: The AutoVision vehicle platform.

ping as we want to leverage a 3D geometric map to do terrain traversability analysis and handle negative obstacles and rough terrain, and facilitate navigation of multi-level structures. In addition, fusing image segmentation results into a 3D geometric map allows us to obtain a consistent 3D semantic map which can be useful for handling navigation in complex environments such as dirt tracks with encroaching vegetation. We follow the traditional approach [29, 3] of applying multi-view geometry to localization and 3D geometric mapping, and machine learning to cross-modal matching, object detection, and scene segmentation. On the other hand, with the advent of deep neural networks, people [2] have attempted to use end-to-end learning for vision-based autonomous vehicles but with limited success.

II. SYSTEM

In this section, we give an overview of the sensors on the AutoVision vehicle platform, and the software architecture that enables various software modules to work together to enable the vehicle to localize and perceive in 3D.

A. Hardware

Our AutoVision vehicle platform is a Isuzu D-Max pickup truck which has been modified to include a drive-by-wire system for autonomous driving. Fig. 1 shows the vehicle platform while Fig. 2 shows a close-up view of the sensors on the vehicle roof. 4 color cameras and 12 NIR cameras are fitted with fisheye lenses and installed in a surround-view configuration on top of the vehicle. All cameras output 2-megapixel images at 30 Hz, and are set to automatic exposure mode so that they can adapt to changing lighting conditions.

¹DSO National Laboratories

²ETH Zürich

³MPI-IS and University of Tübingen

⁴National University of Singapore



Fig. 2: A close-up of the sensor suite on the AutoVision vehicle platform.

We only use 12-bit grayscale images from the NIR cameras as input to all localization and perception modules. NIR cameras are more light-sensitive than color cameras, and provide sharp and clean images unlike Bayer-encoded color images that suffer from false color artifacts. In addition, NIR cameras are used in conjunction with NIR illuminators which can improve low-light imaging quality and whose illumination is invisible to and does not distract drivers on the road. Fig. 4 shows examples of images captured at approximately the same location in varying lighting conditions. Camera enclosures provide cameras with IP67 protection from the weather elements. Fig. 3 shows the camera layout on the vehicle roof. The front side of the vehicle has the highest number of NIR cameras; these 5 NIR cameras facilitate wide-baseline stereo, and in turn, long-range perception which is critical for autonomous vehicles moving forward at high speeds. We exploit the mostly longitudinal movement of the vehicle by simulating a multi-baseline stereo system on each side of the vehicle and which consists of 2 actual NIR cameras and at least 1 virtual NIR camera.

A dual-antenna GNSS/INS system with a tactical-grade IMU is installed in the vehicle. Data from this GNSS/INS system is post-processed offline to yield centimeter-level ground-truth position and attitude data which is used to evaluate localization accuracy. A 3D LiDAR sensor is mounted at each of the four corners of the vehicle roof; fused point cloud data from all 4 LiDAR sensors is used to evaluate perception accuracy. All sensor data is hardware-timestamped to sub-microsecond precision. Such accurate time synchronization is made possible through the use of a time server which time-synchronizes LiDARs via PPS signals and NMEA data, and cameras via PTP. All sensors interface over a 10 GbE network switch with several industrial-grade computers equipped with GPUs.

B. Software

Our software stack is based on the ROS 2 software framework, and runs on Windows 10. We use RTI Connex DDS for inter-process communications. Fig. 5 shows our software architecture; with the exception of the block representing sparse 3D map reconstruction, each block represents a node which subscribes and publishes to topics.

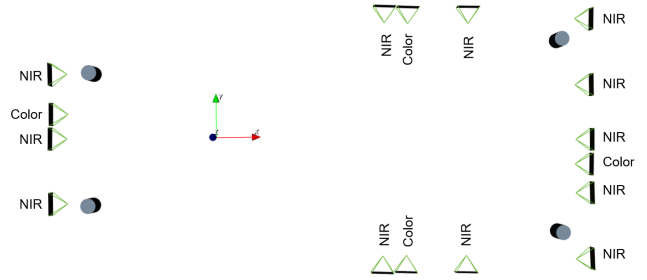


Fig. 3: The sensor layout on the AutoVision vehicle platform. Each green-colored frustum and grey-colored cylinder represent a camera and LiDAR sensor respectively. The origin of the three axes indicates the location of the IMU. The red-colored x -axis points towards the front of the vehicle while the green-colored y -axis points towards the left of the vehicle. The extrinsic transformation between each sensor and the IMU was estimated with automated calibration tools.

III. CALIBRATION

An accurate calibration is an essential prerequisite for localization and perception to work well with a multi-camera system. Automated calibration is done with a set of calibration tools. We do intrinsic and extrinsic calibration of the multi-camera system with the help of a fiducial target which is a grid of AprilTag markers [28] with known dimensions, and is shown in Fig. 6. For this calibration, we can choose from multiple camera projection and distortion models. In this project, we use the unified projection model [9, 1] and the plumb bob distortion model [4]. We also perform a photometric calibration of each camera using the method described in [6]. This photometric calibration is useful for photometric-based matching between images captured with different exposure times, for example, in direct visual odometry and plane-sweeping stereo.

We obtain the extrinsic transformation between the multi-camera system and the IMU by following an approach similar to that of Heng et al. [13, 14]. Here, the reference frame of the IMU coincides with that of the GNSS/INS system. We run semi-direct stereo visual odometry [12] for a stereo pair on each side of the vehicle, run hand-eye calibration with poses from stereo visual odometry and the GNSS/INS system to obtain an initial estimate of the extrinsic transformation, and run non-linear refinement by minimizing the sum of squared reprojection errors from feature tracks while keeping the GNSS/INS system poses and inter-camera transformations fixed.

IV. LOCALIZATION

One goal of Project AutoVision is to enable an autonomous vehicle to localize in both unmapped and premapped environments. A vehicle relying on map-based localization is restricted to movement within the map. We want to allow the vehicle to navigate beyond the map into unmapped areas by leveraging satellite imagery. However, a premapped environment enables the vehicle to localize with



Fig. 4: Images captured from a front left camera on the AutoVision vehicle and in varying lighting conditions.

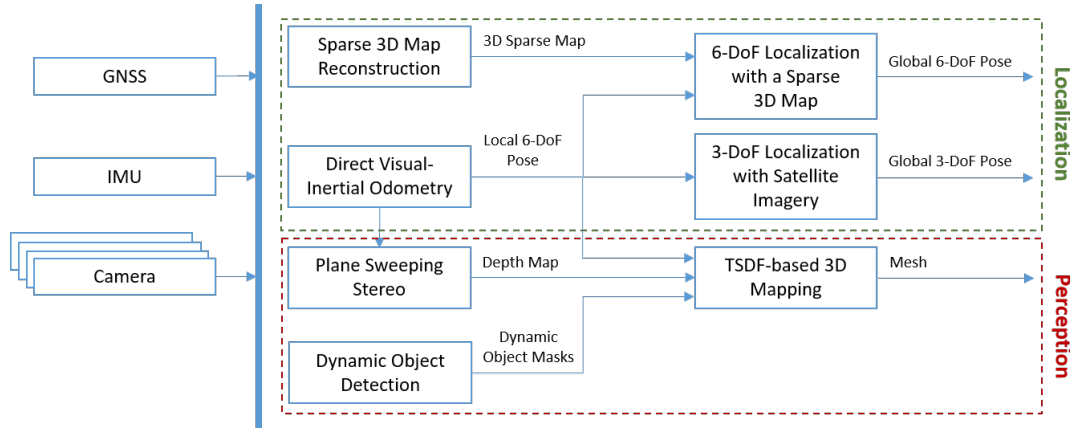


Fig. 5: Our AutoVision software architecture. GNSS is only used for sparse 3D map reconstruction.

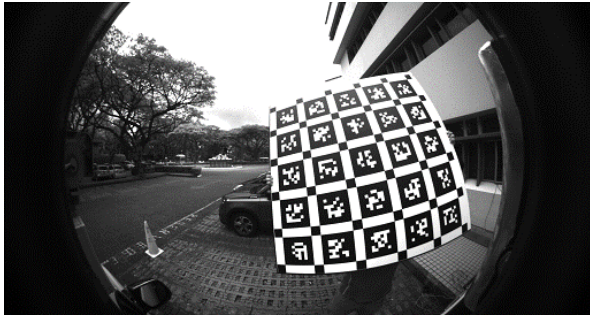


Fig. 6: The fiducial target used for calibration of the multi-sensor system.

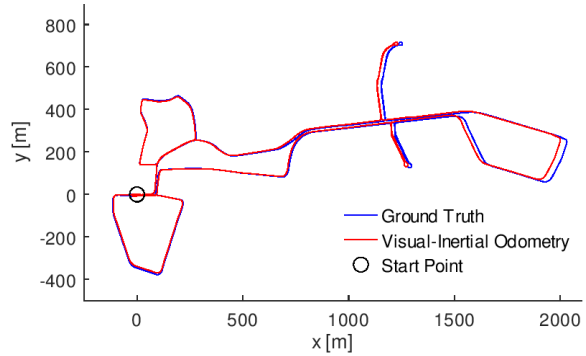


Fig. 7: The positions estimated by VIO vs ground truth positions. One front stereo pair and one rear stereo pair were used for VIO.

higher accuracy. Global pose estimates are susceptible to pose jumps; smooth local pose estimates are required for stable path tracking and to build consistent 3D maps. For this purpose, we use direct visual-inertial odometry which runs at the frame rate of the multi-camera system.

A. Direct Visual-Inertial Odometry

Our direct visual-inertial odometry (VIO) implementation for a multi-camera system [21, 22] estimates the local pose of the vehicle at 30 Hz. Our direct VIO implementation contains two threads: (1) the tracking thread estimates the local pose by minimizing photometric errors between the most recent keyframe and the current frame, and (2) the mapping thread initializes the depth of all sampled feature points using plane-sweeping stereo, and uses a sliding window optimizer

to refine poses and structure jointly. Extensive experiments described by Liu et al. [22] show our implementation to work robustly for a 4-stereo-camera configuration with less than 1% translational drift in day-time and night-time with NIR illumination, and less than 2% translational drift in night-time without NIR illumination. Fig. 7 plots the pose estimates from our VIO implementation against ground truth data for a 8.2km route in a route covering both urban and rural environments.

B. 3-DoF Localization with Satellite Imagery

In areas that have not been premaped, we rely on satellite imagery to estimate the 3-DoF global pose. Specifically, we estimate the (x, y) position and heading of the vehicle with

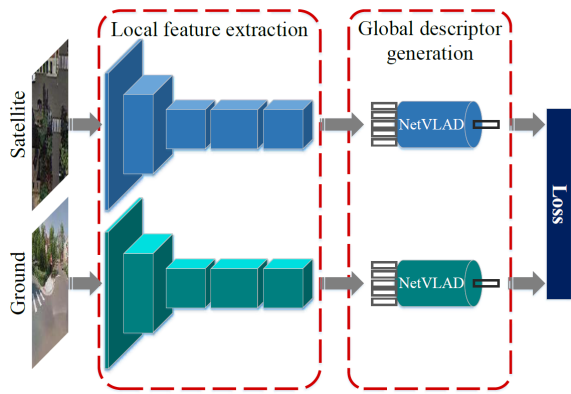


Fig. 8: The architecture of our deep network, CVM-Net, for cross-view matching.

respect to the UTM coordinate frame. Assuming that the starting position and heading are initially known, we use the particle filter approach in which we use local pose data from VIO for particle propagation and output from a deep network [15] for particle weighting.

As shown in Fig. 8, the deep network called CVM-Net is a Siamese network that takes satellite and ground-level panoramic images as input. We obtain the panoramic image by stitching the cylindrical projections of images taken from four cameras: one camera on each side of the vehicle. For each image, we extract local features via fully convolutional networks. Two aligned NetVLADs aggregate local features from both images into global descriptors that are in a common space for similarity comparison. The weight for each particle is inversely proportional to the Euclidean distance between the global descriptors corresponding to the ground-level panoramic image and the satellite image patch nearest the particle’s position.

We run two experiments with a 5km route in both an urban environment and a rural environment. Experimental results show that our satellite-imagery-based localization achieves an average position error of 9.92m and an average heading error of 0.32° over a 5km route in the urban environment, and an average position error of 9.29m and an average heading error of 0.42° in the rural environment. Fig. 9 visualizes our satellite-imagery-based localisation in an urban environment. The top left image shows the ground-view panoramic image. The bottom left image shows the paths estimated by our localization and GNSS/INS system in green and red respectively on the bottom left. In the right image, particles are shown in blue on the right and interposed against a likelihood map; the more red the pixel, the higher the likelihood that the vehicle is located at that pixel.

C. Sparse 3D Map Reconstruction

Sparse 3D map reconstruction is required for map-based 6-DoF localization which is described in Section IV-D. Prior to localization, we build a sparse 3D map in which each 3D point is associated with one or more local SIFT features [23].

To minimize the time required for large-scale reconstruction, our approach does not reconstruct the scene from

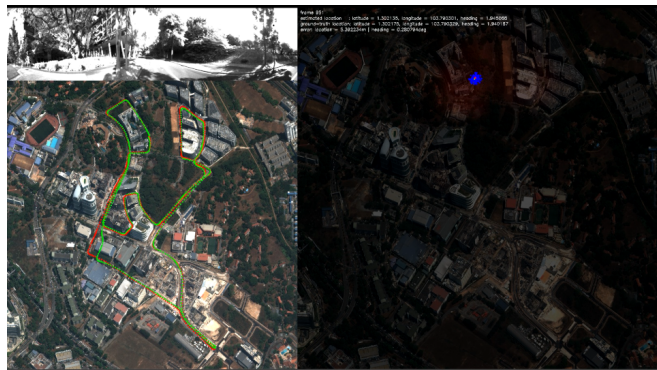
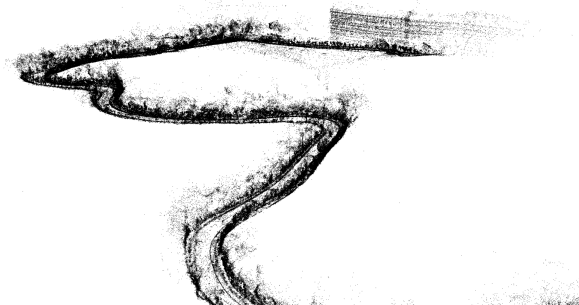


Fig. 9: A visualization of our satellite-imagery-based localisation in an urban environment.



(a) A sparse 3D map of an urban environment.



(b) A sparse 3D map of a rural environment.

Fig. 10: The sparse 3D maps generated by our reconstruction pipeline.

scratch, and instead, uses reasonably accurate initial pose estimates from a GNSS/INS system to initialize all camera poses. In addition, we require a minimum amount of camera motion between images used for mapping. Next, we perform feature matching between nearby images, and use the feature matches and initial poses to triangulate the scene. We then repeatedly optimize the scene structure and camera poses using bundle adjustment followed by the merging of feature tracks. This approach is implemented on top of the COLMAP structure-from-motion (SfM) framework [26]. During bundle adjustment, we enforce that the extrinsic parameters of the multi-camera system on the AutoVision vehicle remain constant. Fig. 10 shows sparse 3D maps of urban and rural environments.

D. 6-DoF Localization with a Sparse 3D Map

Given a sparse 3D map computed using the approach described in Section IV-C and without prior knowledge of the AutoVision vehicle’s global pose, we localize the

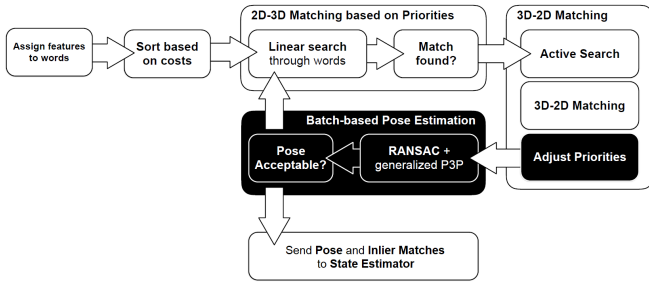


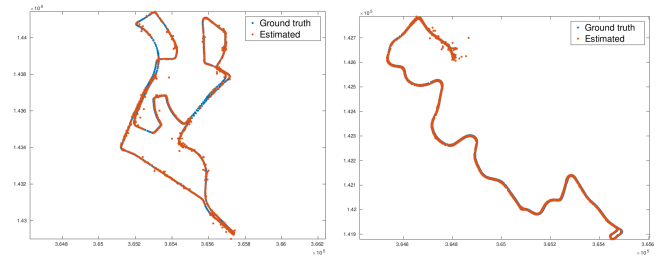
Fig. 11: The localization pipeline used in Project AutoVision. White boxes denote components based on the Active Search approach from [25]. Black boxes correspond to our modifications made to adapt to the multi-camera system used in Project AutoVision.

AutoVision vehicle by extracting local SIFT features [23] from the images captured by the cameras mounted on the AutoVision vehicle and matching the descriptors of these 2D features against the descriptors associated with the 3D points in the map. From the 2D-3D matches, we apply a generalized perspective-n-point pose solver [18, 19] inside a RANSAC loop [7] to both estimate the vehicle pose and identify inliers. These outputs are then passed to the state estimator described in Section IV-E. Fig. 11 illustrates our localization pipeline. With a sparse 3D map of a large area which contains many 3D points, 2D-3D matching is the main computational bottleneck in our pipeline. In this case, we use a prioritized matching approach based on Active Search [25] for improved matching efficiency.

Active Search is based on two core principles: prioritized descriptor matching and combining 2D-to-3D and 3D-to-2D matching. In an offline step, Active Search assigns each 3D point descriptor in the sparse 3D map to its closest visual word from a pre-defined visual vocabulary. It then computes the search cost for each word by counting the number of 3D points with descriptors assigned to that word.

Given all images captured at the same time by the multi-camera system, we first extract local SIFT features and then assign each feature to its closest visual word. Active Search first tries to find matches for features assigned to words containing only few 3D points and progressively considers features that are more and more expensive to match. 2D-to-3D correspondence search is then terminated once a fixed number of matches is found. The disadvantage of this prioritization scheme is that assigning descriptors to visual words leads to quantization artifacts. These artifacts occur when the descriptors of a feature and its corresponding 3D point are mapped to different visual words. In order to recover matches lost to such artifacts, Active Search employs a 3D-to-2D matching step: if the correspondence between a feature f and its matching 3D point p is correct, then it is highly likely that other 3D points around p are also visible in the query image. These candidates are then matched against the features in the query image using a smaller visual vocabulary.

As shown in [25], finding so many matches in a small region in the query image leads to unstable configurations for pose estimation. However, as long as correspondences are



(a) Urban environment. In some parts of the area, the localization fails consistently to estimate a pose. (b) Rural environment. The errors at the top end are likely caused by repetitive structures on both sides of the road.

Fig. 12: The positions estimated by map-based localization vs. ground truth positions for a 5km route in two different environments.

found in multiple images from the multi-camera system, the geometric configuration of the matches is still stable enough to allow accurate pose estimation. In addition, we ensure that the algorithm finds matches in multiple images by modifying the prioritized search to first find a few matches in all images before finding the rest of the matches.

For our experiments, we use the same routes used for the satellite-imagery-based localization experiments described in Section IV-B. Our localization pipeline runs at around 2 Hz on the AutoVision vehicle. Fig. 12 shows the estimated and ground truth positions for the urban and rural routes. For the urban route, the mean and median errors of all reported poses are 3.31m and 1.84m for the position, and 2.6° and 1.9° for the heading, respectively. For the rural route, the mean and median errors of all reported poses are 3.48m and 1.81m for the position, and 4.2° and 3.3° for the heading, respectively.

E. State Estimator

Our VIO implementation estimates accurate local vehicle motions at the full frame rate of the multi-camera system. However, the estimated vehicle poses are not reliable for long-term operation due to drift. In contrast, map-based localization provides less accurate but long-term consistent pose estimates at around 2 Hz. Therefore, in the state estimator, we integrate outputs from VIO and map-based localization to provide accurate, drift-free vehicle poses at the full frame rate.

We initialize the first vehicle pose node of the factor graph with the estimated pose from the map-based localization. We create a new vehicle pose node each time we have new measurements from the localization. Since VIO runs at a much higher rate than the localization, we concatenate all VIO measurements within the time interval of two consecutive pose nodes to constrain their relative pose. The 2D-3D feature correspondences provided by the localization component are then used to constrain the global vehicle poses in terms of reprojection errors. We optimize the factor graph each time the localization provides new measurements. Vehicle poses are computed at the full frame rate by integrating relative

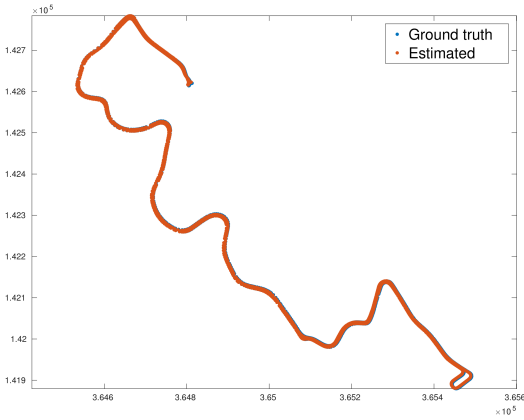


Fig. 13: The positions estimated by our state estimator vs. ground truth positions for a 5km route in a rural environment.

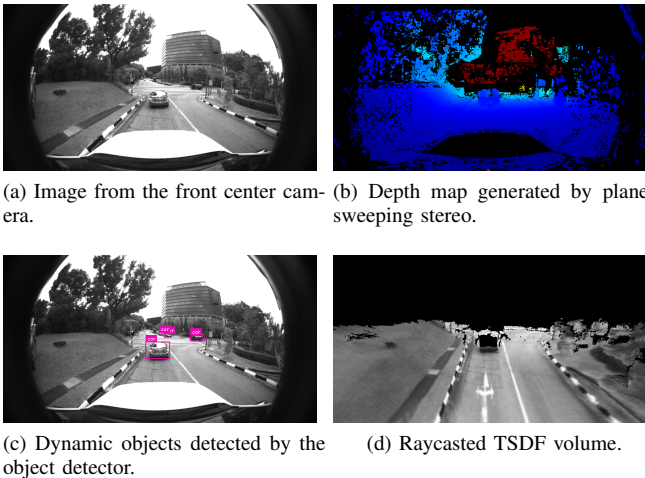


Fig. 14: Output from the AutoVision perception modules.

poses estimated by VIO with respect to the latest vehicle pose node of the factor graph.

Fig. 13 shows the estimated and ground truth positions for the rural route. Compared to the pure map-based localization results shown in Fig. 12b, all localization errors at the top end are removed.

V. PERCEPTION

For an autonomous vehicle to navigate in complex environments, we need to generate a dense 3D map of its environment in 3D and in real-time. Plane-sweeping stereo generates depth maps which are fused into a truncated signed distance function (TSDF) volume. A 3D map is reconstructed from this TSDF volume via ray-casting. To avoid dynamic objects leaving artifacts on the map, we use an object detector to detect dynamic objects and estimate their bounding boxes which are used to mask out areas in depth images corresponding to dynamic objects prior to depth map fusion. Fig. 14 visualizes the outputs from plane-sweeping stereo, object detection, and TSDF-based 3D mapping.

A. Plane-Sweeping Stereo

Plane-sweeping stereo computes a depth map for multiple images with known camera poses by sweeping a set of planes through 3D space. Each plane represents a depth hypothesis and defines a homography mapping from every other view to the reference view. We estimate the depth for each pixel in a reference image by using each plane to warp each non-reference image to the reference image, evaluating the image dissimilarity at that pixel, and choosing the plane that minimizes the image dissimilarity. We use the GPU implementation of plane-sweeping stereo for fisheye cameras [10] which computes depth maps directly from fisheye images without the need for undistortion, allowing us to use the full field-of-view of the cameras. On the AutoVision vehicle, plane-sweeping stereo runs at an average of 15 Hz for the 5 cameras at the front of the vehicle and with images downsampled to half-resolution.

B. TSDF-based 3D Mapping

The depth maps only maintain local geometric information, and we need to fuse depth maps estimated at different positions in time into a single 3D map for more informed perception. We use a standard fusion technique: the scene is represented via a set of voxels where each voxel stores a TSDF value [5]. Thus, each voxel stores the signed distance to the closest object surface (negative inside of objects, positive outside of objects, zero on surfaces), truncated to a certain maximum / minimum value. Whenever a new depth image along with its camera pose becomes available, we update the 3D model. We use the map fusion pipeline in the InfiniTAM library [16, 17]. We also use the fast raycasting algorithm in [16, 17] to reconstruct the 3D map in the current camera view. The pipeline runs at around 20 Hz on the AutoVision vehicle.

C. Dynamic Object Detection

We use the YOLOv3 object detection network [24] with pre-trained weights from the Microsoft COCO dataset [20]. This dataset contains undistorted color images and contains 80 object classes, most of which are not relevant to autonomous driving. In contrast, our NIR cameras with fisheye lenses provide distorted grayscale images, and we only want to differentiate between static and dynamic objects. We fine-tune the network by truncating the first and last layers, and retrain the network using our labeled datasets.

VI. CONCLUSIONS

Project AutoVision has successfully demonstrated localization and 3D scene perception for autonomous vehicles with multi-camera systems, in both urban and rural environments, and without GNSS. As Project AutoVision progresses, we will continue to enhance localization and perception capabilities, and add more modules to our software stack. These modules include but are not limited to, change detection for 3D maps, obstacle detection, dynamic object tracking and classification, and semantic 3D mapping.

REFERENCES

- [1] J. Baretto and H. Araujo. Issues on the geometry of central catadioptric image formation. In *IEEE Conference on Computer Vision and Pattern Recognition (CVPR)*, 2001.
- [2] M. Bojarski, D. D. Testa, D. Dworakowski, B. Firner, B. Flepp, P. Goyal, L. D. Jackel, M. Monfort, U. Muller, J. Zhang, X. Zhang, J. Zhao, and K. Zieba. End to end learning for self-driving cars. *CoRR*, abs/1604.07316, 2016.
- [3] A. Broggi, P. Cerri, S. Debattisti, M. C. Laghi, P. Medici, D. Molinari, M. Panciroli, and A. Prioletti. Proudpublic road urban driverless-car test. *IEEE Transactions on Intelligent Transportation Systems*, 16(6):3508–3519, 2015.
- [4] D. C. Brown. Decentering distortion of lenses. *Photometric Engineering*, 32(3):444–462, 1966.
- [5] B. Curless and M. Levoy. A volumetric method for building complex models from range images. In *Annual Conference on Computer Graphics and Interactive Techniques (SIGGRAPH)*, 1996.
- [6] J. Engel, V. C. Usenko, and D. Cremers. A photometrically calibrated benchmark for monocular visual odometry. *CoRR*, abs/1607.02555, 2016.
- [7] M. A. Fischler and R. C. Bolles. Random sample consensus: a paradigm for model fitting with applications to image analysis and automated cartography. *Communications of the ACM*, 24:381395, 1981.
- [8] P. Furgale, U. Schwesinger, M. Ruffli, W. Derendarz, H. Grimmert, P. Mühlfellner, S. Wonneberger, J. Timpner, S. Rottmann, B. Li, B. Schmidt, T. N. Nguyen, E. Cardarelli, S. Cattani, S. Brüning, S. Horstmann, M. Stellmacher, H. Mielenz, K. Köser, M. Beermann, C. Häne, L. Heng, G. H. Lee, F. Fraundorfer, R. Iser, R. Triebel, I. Posner, P. Newman, L. Wolf, M. Pollefeys, S. Brosig, J. Effertz, C. Pradalier, and R. Siegwart. Toward automated driving in cities using close-to-market sensors: An overview of the v-charge project. In *IEEE Intelligent Vehicles Symposium (IV)*, 2013.
- [9] C. Geyer and K. Daniilidis. A unifying theory for central panoramic systems and practical implications. In *European Conference on Computer Vision (ECCV)*, 2000.
- [10] C. Häne, L. Heng, G. H. Lee, A. Sizov, and M. Pollefeys. Real-time direct dense matching on fisheye images using plane-sweeping stereo. In *International Conference on 3D Vision (3DV)*, 2015.
- [11] C. Häne, L. Heng, G. H. Lee, F. Fraundorfer, P. Furgale, T. Sattler, and M. Pollefeys. 3d visual perception for self-driving cars using a multi-camera system: Calibration, mapping, localization, and obstacle detection. *Image and Vision Computing (IVC)*, 68:14–27, 2017.
- [12] L. Heng and B. Choi. Semi-direct visual odometry for a fisheye-stereo camera. In *IEEE/RSJ International Conference on Intelligent Robots and Systems (IROS)*, 2016.
- [13] L. Heng, P. Furgale, and M. Pollefeys. Leveraging image-based localization for infrastructure-based calibration of a multi-camera rig. *Journal of Field Robotics (JFR)*, 32:775–802, 2015.
- [14] L. Heng, G. H. Lee, and M. Pollefeys. Self-calibration and visual slam with a multi-camera system on a micro aerial vehicle. *Autonomous Robots (AURO)*, 39:259–277, 2015.
- [15] S. Hu, M. Feng, R. M. H. Nguyen, and G. H. Lee. Cvmmnet: Cross-view matching network for image-based ground-to-aerial geo-localization. In *IEEE Conference on Computer Vision and Pattern Recognition (CVPR)*, 2018.
- [16] O. Kähler, V. A. Prisacariu, C. Y. Ren, X. Sun, P. Torr, and D. Murray. Very high frame rate volumetric integration of depth images on mobile devices. *IEEE Transactions on Visualization and Computer Graphics (TVCG)*, 21(11):1241–1250, 2015.
- [17] O. Kähler, V. Prisacariu, J. Valentin, and D. Murray. Hierarchical voxel block hashing for efficient integration of depth images. *IEEE Robotics and Automation Letters (RA-L)*, 1(1):192–197, 2016.
- [18] L. Kneip, P. Furgale, and R. Siegwart. Using multi-camera systems in robotics: Efficient solutions to the npnp problem. In *IEEE International Conference on Robotics and Automation (ICRA)*, 2013.
- [19] G. H. Lee, B. Li, M. Pollefeys, and F. Fraundorfer. Minimal solutions for the multi-camera pose estimation problem. *International Journal of Robotics Research (IJRR)*, 34:837–848, 2015.
- [20] T.-Y. Lin, M. Maire, S. Belongie, J. Hays, P. Perona, D. Ramanan, P. Dollár, and C. L. Zitnick. Microsoft coco: Common objects in context. In *European Conference on Computer Vision (ECCV)*, 2014.
- [21] P. Liu, L. Heng, T. Sattler, A. Geiger, and M. Pollefeys. Direct visual odometry for a fisheye-stereo camera. In *IEEE/RSJ International Conference on Intelligent Robots and Systems (IROS)*, 2017.
- [22] P. Liu, M. Geppert, L. Heng, T. Sattler, A. Geiger, and M. Pollefeys. Towards robust visual odometry with a multi-camera system. In *IEEE/RSJ International Conference on Intelligent Robots and Systems (IROS)*, 2018.
- [23] D. G. Lowe. Distinctive image features from scale-invariant keypoints. *International Journal of Computer Vision (IJCV)*, 60(2):91110, 2004.
- [24] J. Redmon and A. Farhadi. Yolov3: An incremental improvement. *CoRR*, abs/1804.02767, 2018.
- [25] T. Sattler, B. Leibe, and L. Kobbelt. Efficient & effective prioritized matching for large-scale image-based localization. *IEEE Transactions on Pattern Analysis and Machine Intelligence (PAMI)*, 39:17441756, 2017.
- [26] J. Schönberger and J. Frahm. Structure-from-motion revisited. In *IEEE Conference on Computer Vision and Pattern Recognition (CVPR)*, 2016.
- [27] U. Schwesinger, M. Bürki, J. Timpner, S. Rottmann, L. Wolf, L. M. Paz, H. Grimmert, I. Posner, P. Newman,

- C. Häne, L. Heng, G. H. Lee, T. Sattler, M. Pollefeys, M. Allodi, F. Valenti, K. Mimura, B. Goebelsmann, W. Derendarz, P. Mühlfellner, S. Wonneberger, R. Waldmann, S. Grysczyk, C. Last, S. Brüning, S. Horstmann, M. Bartholomäus, C. Brummer, M. Stellmacher, F. Pucks, M. Nicklas, and R. Siegwart. Automated valet parking and charging for e-mobility. In *IEEE Intelligent Vehicles Symposium (IV)*, 2016.
- [28] J. Wang and E. Olson. AprilTag 2: Efficient and robust fiducial detection. In *IEEE/RSJ International Conference on Intelligent Robots and Systems (IROS)*, 2016.
- [29] J. Ziegler, P. Bender, M. Schreiber, H. Lategahn, T. Strauss, C. Stiller, T. Dang, U. Franke, N. Appenrodt, C. G. Keller, E. Kaus, R. G. Herrtwich, C. Rabe, D. Pfeiffer, F. Lindner, F. Stein, F. Erbs, M. Enzweiler, C. Knoppel, J. Hipp, M. Haueis, M. Trepte, C. Brenk, A. Tamke, M. Ghanaat, M. Braun, A. Joos, H. Fritz, H. Mock, M. Hein, and E. Zeeb. Making bertha drive - an autonomous journey on a historic route. *IEEE Intelligent Transportation Systems Magazine*, 6(2):8–20, 2014.